
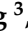

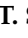

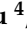
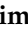




Surface Electronic Structure of Cr Doped Bi₂Se₃ Single Crystals

Turgut Yilmaz ^{1,2,*} , Xiao Tong ³ , Zhongwei Dai ³ , Jerzy T. Sadowski ³ , Genda Gu ⁴ , Kenya Shimada ⁵ , Sooyeon Hwang ³ , Kim Kisslinger ³ , Elio Vescovo ¹ and Boris Sinkovic ² 

¹ National Synchrotron Light Source II, Brookhaven National Laboratory, Upton, NY 11973, USA; vescovo@bnl.gov

² Department of Physics, University of Connecticut, Storrs, CT 06269, USA; boris.sinkovic@uconn.edu

³ Center for Functional Nanomaterials, Brookhaven National Lab, Upton, NY 11973, USA; xtong@bnl.gov (X.T.); zhongwei@lbl.gov (Z.D.); sadowski@bnl.gov (J.T.S.); soohwang@bnl.gov (S.H.); kisslinger@bnl.gov (K.K.)

⁴ Condensed Matter Physics and Materials Science Department, Brookhaven National Lab, Upton, NY 11973, USA; ggu@bnl.gov

⁵ Hiroshima Synchrotron Radiation Center, Hiroshima University, 2-313 Kagamiyama, Higashihiroshima 739-0046, Japan; kshimada@hiroshima-u.ac.jp

* Correspondence: trgt2112@gmail.com

Abstract: Here, by using angle-resolved photoemission spectroscopy, we showed that Bi_{2-x}Cr_xSe₃ single crystals have a distinctly well-defined band structure with a large bulk band gap and undistorted topological surface states. These spectral features are unlike their thin film forms in which a large nonmagnetic gap with a distorted band structure was reported. We further provide laser-based high resolution photoemission data which reveal a Dirac point gap even in the pristine sample. The gap becomes more pronounced with Cr doping into the bulk of Bi₂Se₃. These observations show that the Dirac point can be modified by the magnetic impurities as well as the light source.

Keywords: topological insulators; ferromagnetism; surface states; angle-resolved photoemission spectroscopy



Citation: Yilmaz, T.; Tong, X.; Dai, Z.; Sadowski, J.T.; Gu, G.; Shimada, K.; Hwang, S.; Kisslinger, K.; Vescovo, E.; Sinkovic, B. Surface Electronic Structure of Cr Doped Bi₂Se₃ Single Crystals. *Crystals* **2024**, *14*, 812. <https://doi.org/10.3390/cryst14090812>

Academic Editor: Omar Chmaissem

Received: 18 August 2024

Revised: 2 September 2024

Accepted: 12 September 2024

Published: 14 September 2024



Copyright: © 2024 by the authors. Licensee MDPI, Basel, Switzerland. This article is an open access article distributed under the terms and conditions of the Creative Commons Attribution (CC BY) license (<https://creativecommons.org/licenses/by/4.0/>).

1. Introduction

Topological insulators (TIs) gained great attention due to their peculiar electronic structure characterized by strong spin-orbit coupling [1,2]. These materials are insulating in the bulk while hosting metallic topological surface states (TSSs) with a chiral spin texture at the boundary. TSSs are described by the massless Dirac equation and are protected against non-magnetic perturbations by time-reversal symmetry (TRS) [1,2]. Novel magnetic states of matter can be realized in TIs through the interaction between the TSSs and the internal magnetic exchange field. In particular, the ferromagnetic order can break TRS and open a magnetic gap at the Dirac point (DP) by lifting the spin degeneracy, and hence the dissipationless chiral edge state propagating along the sample edge can emerge without the need for the external magnetic field [3,4]. Such a state of matter is known as the quantum anomalous Hall effect (QAHE). Accordingly, the QAHE was experimentally realized in V- and Cr-doped (Bi, Sb)₂Te₃ thin films, but at temperatures far below the ferromagnetic transition temperature [5,6]. Since then, there have been intensive studies to resolve these obstacles and increase the onset temperature for the QAHE. It has been recognized that the fundamental drawbacks are the dopant-induced disorder in the lattice and unfavorable distortion of the band structure [7–13]. So far, most of the transport and photoemission experiments have been conducted on magnetic topological insulators (MTIs) prepared as thin films, based on the expectation that the thinner samples can be less disordered. This has made molecular beam epitaxy (MBE) a primary technique to grow MTI materials. However, MBE may not be an ideal method to prepare MTIs because of the low growth temperature required for chalcogenides which may form the clustering of dopants. On the other hand, abundant vacancies form at high growth temperatures which can induce disorders and

strongly modify the chemical potential of the system [14]. Therefore, fabricating MTIs with the lowest density of defects and desired electronic structure is still one of the critical steps in facilitating future studies and applications. Among many TIs, Bi_2Se_3 is one of the most promising systems due to its simple electronic structure with a large bulk band gap where the DP is located [2]. This leads to extensive theoretical studies of the impact of transition metal doping on its magnetic and electronic structures. However, dopants induce a prominent lifetime broadening in ARPES spectra of Bi_2Se_3 which makes it difficult to catch the details of the band structure [9–13]. Therefore, experimental studies have often adopted (Bi,Sb)Te-based TIs. However, in this material, an unavoidable bulk band crossing at the binding energy of the DP causes non-trivial magnetic quantum states to appear only below a few K [15]. On the other hand, a more robust surface electronic structure and high crystalline quality of Bi_2Se_3 could make it a promising pathway to the realization of a high-temperature QAHE.

Unlike the thin film samples, there are only a few band structure studies on magnetic-impurity-doped Bi_2Se_3 single crystals [16] although their magnetic and transport properties are investigated in more detail [17–19]. In this article, we study the electronic structure of Cr-doped Bi_2Se_3 single crystals grown using the floating zone method. We confirmed their high crystal quality by performing high-angle annular dark-field (HAADF) scanning transmission electron microscopy (STEM), X-ray photoemission spectroscopy (XPS), and micro-spot low energy electron diffraction (μLEED) experiments. Our angle-resolved photoemission spectroscopy (ARPES) experiments show that the surface electronic structure of Cr-doped Bi_2Se_3 single crystals is free of large Dirac gaps and significant lifetime broadening. These enhanced structural and electronic features facilitate the study of the Dirac cone in detail. Hence, our synchrotron-based ARPES experiments show that Bi_2Se_3 has robust gapless surface states against Cr doping. On the other hand, the same samples exhibit a Dirac gap even in the pristine form when the electronic structure is recorded with a laser source and the gap can be further modified with Cr doping. This interesting observation reveals an interplay mechanism between magnetic impurities, light source, and the Dirac cone electronic structure.

2. Materials and Methods

Single crystals with nominal composition $\text{Bi}_{1-x}\text{Cr}_x\text{Se}_3$ were grown by a modified floating-zone method. Bi, Se, and Cr of 6N purity were loaded into double-walled quartz ampules and sealed under vacuum. The materials first were melted at 900 °C in a box furnace and fully rocked to achieve a homogeneous mixture. A 12 mm diameter pre-melted ingot rod in a sealed quartz tube was mounted in a floating-zone furnace in which the pre-melted ingot rod was first pre-melted at a velocity of 200 mm/hr and then grown at 1.0 mm/hr. ARPES experiments were performed at 21-ID-1 ESM beamline of National Synchrotron Light Source II (NSLS-II) by using a DA30 Scienta electron spectrometer (Scienta Omicron, Uppsala, Sweden). The pressure in the photoemission chamber was 1×10^{-10} Torr and samples were kept at 15 K during the experiment by a closed-cycle He cryostat. The angle between the incident beam and the surface normal of the sample at normal emission was 55°. Incident beam spot-size was set to be $\sim 10 \times 10 \mu\text{m}^2$. Single crystals were cleaved in the ARPES chamber at 15 K. High symmetry points in the BZ were calculated by using the free electron final state approximation $\hbar k_z = \sqrt{2m_e(E_{\text{kin}}\cos^2\theta + V_o)}$ where m_e is the free electron mass, E_{kin} is the kinetic energy of a photoelectron, and V_o is the inner potential which is 11.8 eV for Bi_2Se_3 [20]. The laser ARPES experiments were carried out with $h\nu = 6.3$ eV and R4000 Scienta electron spectrometer (Uppsala, Sweden) at the Hiroshima Synchrotron Radiation Center (HiSOR) [21]. Samples were cleaved in ARPES chamber and experiments were conducted at 11 K. XPS experiments were carried out in an ultrahigh vacuum (UHV) system with base pressures $< 2 \times 10^{-9}$ Torr equipped a SPECS, PHOIBOS 100 (Berlin, Germany) hemispherical electron energy analyzer and twin anode X-ray source (SPECS, XR50) (Berlin, Germany). Mg K_α (1253.6 eV) radiation was used at 10 kV and 30 mA. The angle between the analyzer and X-ray source was 45° and photoelectrons were

collected along the sample surface normal. The total experimental resolution in XPS was ~ 1 eV. Depth profile XPS was carried out by sputtering the sample at room temperature. Then, the sample was annealed at 225 °C for 30 min after each sputtering. Sputtering was performed by using SPECS PU-IQE 11/35 (Berlin, Germany) sputtering at 1 W power and $P_{Ar} = 2 \times 10^{-5}$ Torr in the experimental chamber. The sputtering rate was calibrated as 2 Å/min. The magnetic properties of the crystals were measured by using a superconducting quantum interference device (SQUID) (San Diego, CA, USA) at Condensed Matter Physics and Materials Science Department, Brookhaven National Laboratory. HAADF-STEM images were acquired with dedicated Hitachi HD2700C (Hitachi, Tokyo, Japan) STEM with a probe Cs corrector operating at 200 kV at room temperature. Samples were prepared using the in situ lift-out method on the FEI Helios 600 Nanolab dual-beam FIB (Peabody, MA, USA). Final milling was completed at 2 keV. HAADF-STEM experiments were conducted at the Center for Functional Nanomaterials, Brookhaven National Laboratory. μ LEED experiment was performed at XPEEM/LEEM endstation of the ESM beamline (21-ID-2). Samples were cleaved in air and rapidly loaded into the system.

3. Results

We present a HAADF-STEM image of the $\text{Bi}_{1.78}\text{Cr}_{0.22}\text{Se}_3$ single crystal sample in Figure 1a for structural characterization. The high crystalline quality of the sample is clear in its highly ordered periodically aligned atomic lattices and the van der Waals (vdW) gaps between the individual quintuple layers (QLs). This finding is also supported by sharp diffraction patterns in μ LEED (Figure 1b). In addition to probing the local atomic layered structure using HAADF-STEM and surface structure with μ LEED, we also characterize the local electronic structure with XPS. Figure 1b,c show the core levels of the $\text{Bi}_{1.78}\text{Cr}_{0.22}\text{Se}_3$ single crystal at different depths. The $\text{Bi}^{+3} 5d_{5/2}$ and $\text{Bi}^{+3} 5d_{3/2}$ peaks are located at 25 eV and 28.1 eV, respectively, for the cleaved sample. Furthermore, the Cr $2p_{3/2}$ and $2p_{1/2}$ peaks are located at the 575.6 eV and 585.5 eV binding energies, respectively, corresponding to the Cr^{+3} valence state [13,22]. This indicates the isoelectric substitution of Bi with the Cr atoms. The core levels obtained from the different depths with respect to the cleaved surface do not show any prominent differences in the width or the binding energy which confirms the chemical uniformity of the sample. Also, unlike the case of surface doping in thin films [13], the transition metal incorporation into the bulk does not induce any new local electronic structure evident from the Bi 5d and Cr 2p peak shapes. These findings show the single chemical state of the sample as well as the absence of the Cr impurity clusters.

To investigate the magnetic properties of the Cr-doped Bi_2Se_3 single crystal, we carried out the superconducting quantum interference device (SQUID) magnetometry measurement. Figure 2a depicts the zero-field-cooled (ZFC) and field-cooled (FC) magnetization (M) curves under the 500 Oe applied field (H) for a $\text{Bi}_{1.78}\text{Cr}_{0.22}\text{Se}_3$ single crystal. The plot shows signatures of three magnetic transitions at ~ 160 K (T_1), ~ 120 K (T_2), and ~ 20 K (T_3). This indicates the coexistence of the different magnetic states as seen in $(\text{MnBi}_2\text{Te}_4)$ $(\text{Bi}_2\text{Te}_3)_m$ [23]. It is also noteworthy that the M-T curve does not exhibit the characteristics of Cr_xSe_y compounds and/or Cr clusters [24,25]. This suggests that the magnetic responses are the intrinsic property of the sample. Moreover, the M-H curves of the $\text{Bi}_{1.78}\text{Cr}_{0.22}\text{Se}_3$ single crystal at 10 K, 100 K, and 150 K are given in Figure 2b. The expanded scale of M-H curves in the inset of the figure shows a clear hysteresis loop at 10 K. This hysteresis loop weakens at higher temperatures, but it is persistent even at 150 K as a very weak feature suggesting the possible high-temperature ferromagnetic order. Also, M does not saturate even at high fields as an indication for antiferromagnetic or paramagnetic order [26]. Antiferromagnetic TIs are also extremely rare materials which can host axion electrodynamic and quantized magnetoelectric coupling effects. One of the known examples of this class is the recently discovered MnBi_2Te_4 single crystal with a Néel temperature (T_N) of 25.4 K [27]. Furthermore, ferromagnetic order has been observed only in thin films of Cr-doped Bi_2Se_3 [28], while a single crystal of the same sample is antiferromagnetic [19]. The

magnetic order in this film is previously attributed to multimers of several substitutional Cr atoms [29]. Therefore, multiple magnetic transitions and ordering in our sample could be due to the presence of multimer clusters with different arrangements and sizes. Thus, the complex magnetic nature of Cr-doped Bi_2Se_3 single crystals might open possibilities to discover other quantum states in addition to the QAHE.

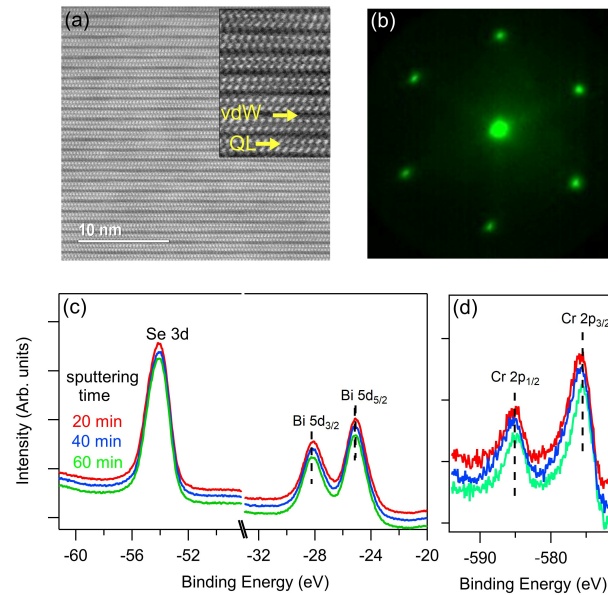


Figure 1. (a) The HAADF-STEM image of the $\text{Bi}_{1.78}\text{Cr}_{0.22}\text{Se}_3$. The inset figure is at a higher magnification. (b) The μLEED pattern of the sample taken with 25 eV electron energy. (c,d) Bi 5d, Se 3d, and Cr 2p core levels of $\text{Bi}_{1.78}\text{Cr}_{0.22}\text{Se}_3$ sample at different depths. All of the data were collected at room temperature.

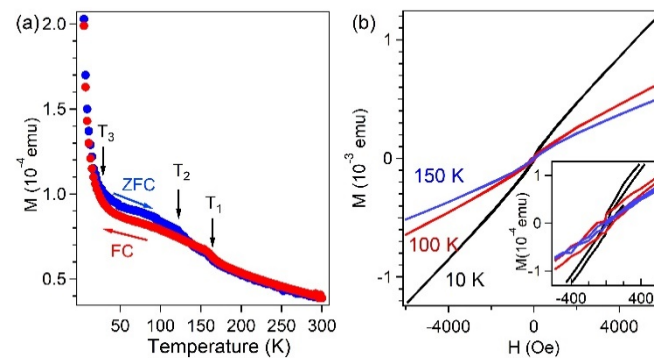


Figure 2. (a) The total out-of-plane magnetic moment is given as a function of temperature for the ZFC and FC processes. During the measurements, 500 Oe is applied. (b) The total magnetic moment versus the applied field at 10 K, 100 K, and 150 K. The inset figure in (b) is the magnified hysteresis in the vicinity of the zero applied field.

In earlier studies, the drastic change in the band structure of a TI due to impurity doping hindered the investigation of the evolution of the TSSs and the bulk bands. In particular, sudden lifetime broadening and an unexpected large gap at the DP were observed in Dy-, V-, Mn-, and Cr-doped Bi_2Se_3 samples grown by MBE [9–13]. On the other hand, the high crystalline quality of the samples studied here can overcome these issues. Figure 3 shows the ARPES momentum (k)–Energy (E) maps of the $\text{Bi}_{2-x}\text{Cr}_x\text{Se}_3$ single crystals for different x values. The pristine Bi_2Se_3 displays the gapless surface Dirac cone with the DP at 0.36 eV binding energy (Figure 3a). The Cr doping does not lead to a prominent modification on the surface electronic structure of Bi_2Se_3 as seen in Figure 3b,c, which show the ARPES maps for $x = 0.1$ and 0.22 . Even though the ferromagnetic order should

open an energy gap at the DP, the energy distribution curves (EDCs) along the $k_x = 0 \text{ \AA}^{-1}$ superimposed in Figure 3 exhibit the DP without a notable energy gap for any doping level. This might be due to the predicted size of the gap of $<10 \text{ meV}$ [30], which is beyond our experimental detection limit. In contrast to our observation, a 50 meV gap at the DP of the $\text{Bi}_{1.993}\text{Cr}_{0.007}\text{Se}_3$ sample is reported in a recent synchrotron-based ARPES study [16]. We will later discuss that the light source is also an effective way of manipulating the DP. Therefore, experimental parameters used in photoemission correlated with the distribution of magnetic impurities could be the main sources of difference. In our samples, the only noticeable impact of Cr doping is a slight downward band bending. This shifts the DP to 0.43 eV binding energy for $x = 0.22$ (Figure 3c). The electron doping can be estimated from the Fermi surface areas enclosed by the TSSs (A_{SS}) and the bulk bands (A_{BB}) [31]. The total charge per surface unit cell is given by $q = (A_{BB} + A_{SS})/A_{BZ}$, where $A_{BZ} = 2.662 \text{ \AA}^{-2}$ is the area of the surface Brillouin zone (BZ) of Bi_2Se_3 . At $x = 0.22$, nearly $\sim 0.013 \text{ e}^-$ per unit cell is transferred from Cr atoms into the surface and the bulk bands. The surface charge density (n_e) is then computed by employing $n_e = q/A_{UC}$, where $A_{UC} = 44.487 \text{ \AA}^2$ is the area of the unit cell of Bi_2Se_3 in real space and n_e is found $\sim 4.3 \times 10^{12} \text{ cm}^{-2}$ for pristine Bi_2Se_3 and $\sim 7.2 \times 10^{12} \text{ cm}^{-2}$ for $\text{Bi}_{1.78}\text{Cr}_{0.22}\text{Se}_3$. The ARPES maps in Figure 3 also allow us to estimate the bulk carrier concentration (n_{3D}) by using the bulk Fermi wave vector k_F where the bulk band crosses the Fermi level. According to $n_{3D} = k_F^3/(3\pi^2)$ and with $k_F = \sim 0.08 \text{ \AA}^{-1}$, n_{3D} is computed as $\sim 1.7 \times 10^{19} \text{ cm}^{-3}$ for $\text{Bi}_{1.78}\text{Cr}_{0.22}\text{Se}_3$.

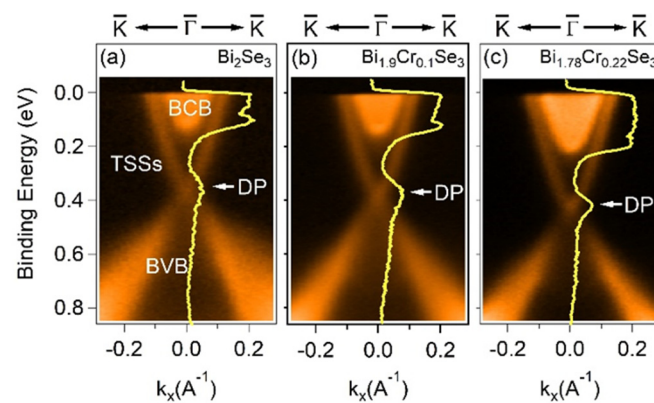


Figure 3. (a–c) ARPES maps of the Bi_2Se_3 , $\text{Bi}_{1.9}\text{Cr}_{0.1}\text{Se}_3$, and $\text{Bi}_{1.78}\text{Cr}_{0.22}\text{Se}_3$ single crystals, respectively. Spectra were observed at 15 K with $h\nu = 30 \text{ eV}$. The superimposed plots are the corresponding EDCs obtained along $k_x = 0 \text{ \AA}^{-1}$.

We also studied the dispersion of the bulk and surface states of the $\text{Bi}_{1.78}\text{Cr}_{0.22}\text{Se}_3$ single crystal along the perpendicular wave vector (k_z) by varying the incident photon energy ($h\nu$); thus, we studied them at different k_z values (Figure 4). TSSs are expected to be k_z -independent due to their 2D nature. This can be seen in the ARPES maps shown in Figure 4a–d where the dispersion remains unchanged under varied $h\nu$. The linear TSSs are also clear in the constant energy cuts of the 3D band structure where they form the circular momentum surfaces (Figure 4e). The dispersions of the bulk bands, however, are modified by the incident $h\nu$. At $h\nu = 30 \text{ eV}$ ($k_z = 3.12 \text{ \AA}^{-1}$) corresponding to the Γ -point, BCB has a maximum at the binding energy of $\sim 0.24 \text{ eV}$, while it is smeared out from the ARPES map at $h\nu = 50 \text{ eV}$ ($k_z = 3.87 \text{ \AA}^{-1}$) corresponding to the Z-point. Similarly, in the k_z -dispersion of BVB, it is also evident that it reaches the minimum binding energy of $\sim 0.6 \text{ eV}$ at $h\nu = 60 \text{ eV}$ ($k_z = 4.2 \text{ \AA}^{-1}$). This gives a large bulk band gap of 0.36 eV where the DP is located. These electronic characteristics are the most important prerequisites for the transport properties to be governed only by TSSs when the DP is pushed to the charge neutral point.

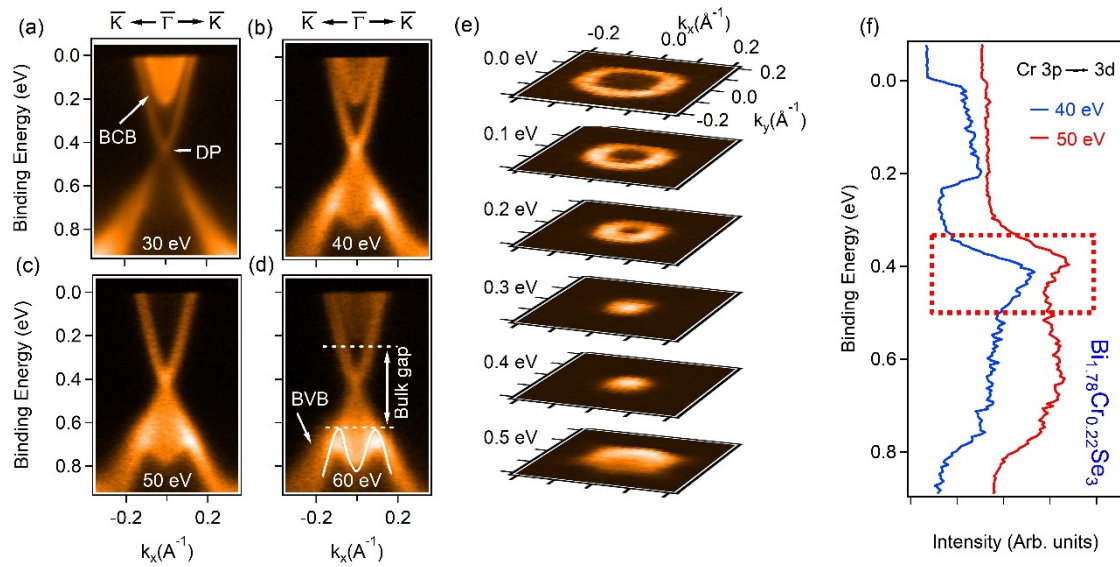


Figure 4. (a–d) The $h\nu$ -dependent experimental electronic structure of the $\text{Bi}_{1.78}\text{Cr}_{0.22}\text{Se}_3$ single crystal obtained with $h\nu = 30$ eV, 40 eV, 50 eV, and 60 eV, respectively. The M-shaped white line in (d) represents the BVB. (e) The constant energy counters at various binding energy taken with $h\nu = 50$ eV. (f) The resonant valence band spectra of $\text{Bi}_{1.78}\text{Cr}_{0.22}\text{Se}_3$ along the $\bar{\Gamma}$ -point at the Cr 3p–3d edge. $h\nu = 40$ eV and $h\nu = 50$ eV are the off- and on-resonant $h\nu$, respectively.

Another advantage of $h\nu$ -dependent ARPES is to identify the impurity states in the band structure. These states can reshape the Dirac cone and even open a non-magnetic gap at the DP [32–35]. To exclude this scenario, we recorded the photoemission spectra of the $\text{Bi}_{1.78}\text{Cr}_{0.22}\text{Se}_3$ single crystal at the Cr resonance. In the resonant photoemission process, core level electrons are photoexcited to empty d-derived states above the Fermi level followed by the relaxation process which resonates with direct d-band photoemission, enhancing the density of states of the d-bands. Figure 4f shows the EDCs taken from the $\text{Bi}_{1.78}\text{Cr}_{0.22}\text{Se}_3$ single crystal both on-resonance ($h\nu = 50$ eV) [36] and off-resonance ($h\nu = 40$ eV) to study the Cr 3p–3d absorption edge. The spectral shape in the vicinity of the DP marked with a dashed red square does not exhibit a prominent modification when $h\nu$ is switched from on- to off-resonant. The only difference between the spectra arises from the k_z dispersion of the bulk bands located above and below the DP. This shows the absence of the Cr 3d impurity states within the energy interval of the DP. However, we should emphasize that Bi_2Se_3 single crystals have been shown to host additional states at the DP for the different dopants which have been proposed by theoretical works [32–35], though the inability to resolve the details of the band structure in current MTI thin films hinders confirmation of these predictions.

Due to the strong distortion on the band structure of the transition-metal-doped TIs, the possible magnetic gap at the DP has not been reliably studied in previous works. These difficulties are not present in the MTI single crystals. Therefore, we searched for the magnetic gap by conducting high-resolution laser-based ARPES experiments from the pristine and Cr-doped Bi_2Se_3 single crystals shown in Figure 5a,b, respectively. The spectral feature of the DP was examined in detail by fitting the EDC cuts obtained along the $\bar{\Gamma}$ point of each spectrum (superimposed in the corresponding figures). Interestingly, the fittings yielded an estimated 16 meV gap even at the DP of the pristine Bi_2Se_3 (Figure 5a). To our knowledge, this anomalous gap was only addressed in TlBiSe_2 TI [8]. One scenario for the non-magnetic gap could be the detachment of the top QLs from the rest of the material during the cleaving which could open a hybridization gap at the DP [37,38]. However, such a scenario would also result in stronger band bending and the formation of quantum well states which we did not observe. Based on our photoemission and structural characterization data, the vacancy-induced modification of the band structure can also be

excluded from being a mechanism for opening a non-magnetic gap [35]. We suggest that it is an intrinsic electronic property of Bi_2Se_3 but the understanding of its nature requires more elaborate and detailed study. Whatever its origin is, it is another fertile parameter to engineer the TSSs, modifying the spin texture of the TSSs in the vicinity of the DP.

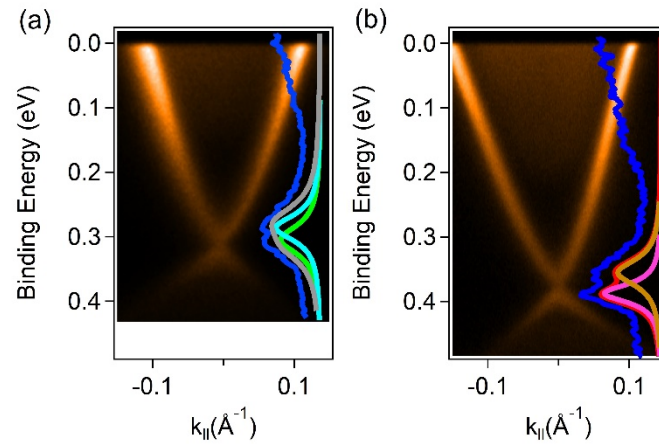


Figure 5. (a,b) ARPES maps of Bi_2Se_3 and $\text{Bi}_{1.78}\text{Cr}_{0.22}\text{Se}_3$ single crystals, respectively. Spectra were recorded with $h\nu = 6.3$ eV laser energy at 12 K. EDCs taken along $k_{\parallel} = 0 \text{ \AA}^{-1}$ are superimposed on each spectrum. Orange, pink, cyan, and green lines are Voigt fitting profiles. Red and grey lines are overall fittings after Shirley backgrounds are subtracted.

We also analyzed the EDC cuts along the $\bar{\Gamma}$ direction in the $\text{Bi}_{1.78}\text{Cr}_{0.22}\text{Se}_3$ ARPES map superimposed in Figure 5b. The Voigt profile fitting of the lower and the upper branch of the DP gives a 30 meV gap at the DP. It is difficult to attribute this gap completely to the magnetic origin since the DP of the pristine sample is already gapped and it is interesting that the gap is not resolved in ARPES experiments conducted with synchrotron radiation at higher photon energies even though the size of the gap for pristine and Cr-doped samples is within our experimental resolution. This suggests that the gap at the DP is correlated with the light source as well as magnetic impurities.

4. Conclusions

In summary, our results reveal that the Cr-doped Bi_2Se_3 single crystals exhibit a well-ordered crystal structure and are free of unexpected distortions on the band structure. We believe that single crystal growth minimizes the dopant clustering and prevents the formation of the other chemical compounds (i.e., Cr_xSe_y). It is also possible to obtain the different structural forms by adopting different growth temperatures and atomic stoichiometry. Similar growth advantages were also utilized in magnetic $(\text{MnBi}) (\text{Bi}_2\text{Te}_3)_m$ self-organized single crystal heterostructures [39]. However, this system still exhibits QAHE only up to a few K, far below the Néel temperature of 23 K [40]. This is possibly due to the bulk band mixing with the TSSs and the involvement of additional symmetry protection of the gapless Dirac cone [41]. Therefore, the absence of these complexities in the surface electronic structure of Bi_2Se_3 makes it one of the most promising candidates for high-temperature QAHE. By taking advantage of the well-defined Dirac cone electronic structure, we have studied the energy gap opening at the DP and found that it exhibits dependence on the photon source and magnetic impurities. Therefore, these results provide new insight into the reshaping of the TSSs in MTIs.

Author Contributions: T.Y. conceived and designed the experiments. G.G. prepared the single crystal samples and performed the magnetic measurements. T.Y., E.V., and B.S. performed the ARPES experiments at NSLS-II. T.Y., E.V., and K.S. performed the ARPES experiments at HiSOR. T.Y. and X.T. conducted the XPS experiments. Z.D. and J.T.S. performed the μLEED measurements. S.H. and K.K. performed the HAADF-STEM experiments. T.Y. analyzed the experimental results and wrote the

manuscript with contributions from B.S. and E.V. All authors have read and agreed to the published version of the manuscript.

Funding: This research received no external funding.

Data Availability Statement: The original contributions presented in the study are included in the article, further inquiries can be directed to the corresponding author.

Acknowledgments: This research used the ESM (21-ID-1, 21-ID-2) beamline of the National Synchrotron Light Source II, a U.S. Department of Energy (DOE) Office of Science User Facility operated for the DOE Office of Science by the Brookhaven National Laboratory under Contract No. DE-SC0012704. This work also used the resources of the Center for Functional Nanomaterials, Brookhaven National Laboratory, which is supported by the U.S. Department of Energy, Office of Basic Energy Sciences, under Contract No. DE-SC0012704. The ARPES experiments in Hiroshima were performed with the approval of the program advisory committee of HiSOR, Proposal No. 19AU003). The author T.Y. would like to thank A.V. Balatsky for useful discussions.

Conflicts of Interest: The authors declare no conflicts of interest.

References

1. Fu, L.; Kane, C.L.; Mele, E.J. Topological insulators in three dimensions. *Phys. Rev. Lett.* **2007**, *98*, 106803. [[CrossRef](#)] [[PubMed](#)]
2. Zhang, H.; Liu, C.X.; Qi, X.L.; Dai, X.; Fang, Z.; Zhang, S.C. Topological insulators in Bi_2Se_3 , Bi_2Te_3 and Sb_2Te_3 with a single Dirac cone on the surface. *Nat. Phys.* **2009**, *5*, 438–442. [[CrossRef](#)]
3. Onoda, M.; Nagaosa, N. Quantized anomalous Hall effect in two-dimensional ferromagnets: Quantum Hall effect in metals. *Phys. Rev. Lett.* **2003**, *90*, 206601. [[CrossRef](#)]
4. Haldane, F.D.M. Model for a quantum Hall effect without Landau levels: Condensed-matter realization of the ‘parity anomaly’. *Phys. Rev. Lett.* **1988**, *61*, 2015–2018. [[CrossRef](#)]
5. Chang, C.Z.; Zhao, W.; Kim, D.Y.; Zhang, H.; Assaf, B.A.; Heiman, D.; Zhang, S.C.; Liu, C.; Chan, M.H.W.; Moodera, J.S. High-precision realization of robust quantum anomalous Hall state in a hard ferromagnetic topological insulator. *Nat. Mater.* **2015**, *14*, 473–477. [[CrossRef](#)]
6. Chang, C.Z.; Zhang, J.; Feng, X.; Shen, J.; Zhang, Z.; Guo, M.; Li, K.; Ou, Y.; Wei, P.; Wang, L.-L.; et al. Experimental observation of the quantum anomalous Hall effect in a magnetic topological insulator. *Science* **2012**, *340*, 167–170. [[CrossRef](#)] [[PubMed](#)]
7. Wray, L.A.; Xu, S.Y.; Xia, Y.; Hsieh, D.; Fedorov, A.V.; Hor, Y.S.; Cava, R.J.; Bansil, A.; Lin, H.; Hasan, M.Z. A topological insulator surface under strong Coulomb, magnetic and disorder perturbations. *Nat. Phys.* **2011**, *7*, 32–37. [[CrossRef](#)]
8. Xu, S.Y.; Neupane, M.; Liu, C.; Zhang, D.; Richardella, A.; Wray, L.A.; Alidoust, N.; Leandersson, M.; Balasubramanian, T.; Sánchez-Barriga, J.; et al. Hedgehog spin texture and Berry’s phase tuning in a magnetic topological insulator. *Nat. Phys.* **2012**, *8*, 616–622. [[CrossRef](#)]
9. Sánchez-Barriga, J.; Varykhalov, A.; Springholz, G.; Steiner, H.; Kirchsclager, R.; Bauer, G.; Caha, O.; Schierle, E.; Weschke, E.; Ünal, A.A.; et al. Nonmagnetic band gap at the Dirac point of the magnetic topological insulator $(\text{Bi}_{1-x}\text{Mn}_x)_2\text{Se}_3$. *Nat. Commun.* **2016**, *7*, 10559. [[CrossRef](#)]
10. Zhang, L.; Zhao, D.; Zang, Y.; Yuan, Y.; Jiang, G.; Liao, M.; Zhang, D.; He, K.; Ma, X.; Xue, Q. Ferromagnetism in vanadium-doped Bi_2Se_3 topological insulator films. *APL Mater.* **2017**, *5*, 076106. [[CrossRef](#)]
11. Harrison, S.E.; Collins-McIntyre, E.J.; Schönherr, P.; Vailionis, A.; Srot, V.; van Aken, P.A.; Kellock, A.J.; Pushp, A.; Parkin, S.S.P.; Harris, J.S.; et al. Massive Dirac fermion observed in lanthanide-doped topological insulator thin films. *Sci. Rep.* **2015**, *5*, 15767. [[CrossRef](#)] [[PubMed](#)]
12. Kou, X.F.; Jiang, W.J.; Lang, M.R.; Xiu, F.X.; He, L.; Wang, Y.; Wang, Y.; Yu, X.X.; Fedorov, A.V.; Zhang, P.; et al. Magnetically doped semiconducting topological insulators. *J. Appl. Phys.* **2012**, *112*, 063912. [[CrossRef](#)]
13. Yilmaz, T.; Hines, W.; Sun, F.C.; Pletikosić, I.; Budnick, J.; Valla, T.; Sinkovic, B. Distinct effects of Cr bulk doping and surface deposition on the chemical environment and electronic structure of the topological insulator Bi_2Se_3 . *Appl. Surf. Sci.* **2017**, *407*, 371–378. [[CrossRef](#)]
14. Yan, B.; Zhang, D.; Felser, C. Topological surface states of Bi_2Se_3 coexisting with Se vacancies. *Phys. Status Solidi RRL* **2012**, *7*, 148. [[CrossRef](#)]
15. Li, W.; Claassen, M.; Chang, C.Z.; Moritz, B.; Jia, T.; Zhang, C.; Rebec, S.; Lee, J.J.; Hashimoto, M.; Lu, D.-H.; et al. Origin of the low critical observing temperature of the quantum anomalous Hall effect in V-doped $(\text{Bi}, \text{Sb})_2\text{Te}_3$ film. *Sci. Rep.* **2016**, *6*, 32732. [[CrossRef](#)]
16. Gardonio, S.; Benher, Z.R.; Fanetti, M.; Moras, P.; Sheverdyeva, P.M.; Valant, M. Single crystal synthesis and surface electronic structure of $\text{Bi}_{1.993}\text{Cr}_{0.007}\text{Se}_3$. *J. Mater. Chem. C* **2024**, *12*, 13236–13241. [[CrossRef](#)]
17. Cermak, P.; Ruleová, P.; Holy, V.; Prokleska, J.; Kucek, V.; Pálka, K.; Benes, L.; Drasar, C. Thermoelectric and magnetic properties of Cr-doped single crystal Bi_2Se_3 —search for energy filtering. *J. Solid State Chem.* **2018**, *258*, 768–775. [[CrossRef](#)]
18. Kulbachinskii, V.A.; Kytin, V.G.; Kudryashov, A.A.; Tarasov, P.M. Thermoelectric properties of Bi_2Te_3 , Sb_2Te_3 and Bi_2Se_3 single crystals with magnetic impurities. *J. Solid State Chem.* **2012**, *193*, 47–52. [[CrossRef](#)]

19. Choi, Y.H.; Jo, N.H.; Lee, K.J.; Yoon, J.B.; You, C.Y.; Jung, M.H. Transport and magnetic properties of Cr-, Fe-, Cu-doped topological insulators. *J. Appl. Phys.* **2011**, *109*, 07E312. [[CrossRef](#)]
20. Bianchi, M.; Guan, D.; Bao, S.; Mi, J.; Iversen, B.B.; King, P.D.C.; Hofmann, P. Coexistence of the topological state and a two-dimensional electron gas on the surface of Bi₂Se₃. *Nat. Commun.* **2010**, *1*, 128. [[CrossRef](#)]
21. Iwasawa, H.; Schwier, E.F.; Arita, M.; Ino, A.; Namatame, H.; Taniguchi, M.; Aiura, Y.; Shimada, K. Development of laser-based scanning μ -ARPES system with ultimate energy and momentum resolutions. *Ultramicroscopy* **2017**, *182*, 85–91. [[CrossRef](#)] [[PubMed](#)]
22. Choi, K.; Lee, S.; Park, J.O.; Park, J.-A.; Cho, S.-H.; Lee, S.Y.; Lee, J.H.; Choi, J.-W. Chromium removal from aqueous solution by a PEI-silica nanocomposite. *Sci. Rep.* **2018**, *8*, 1438. [[CrossRef](#)] [[PubMed](#)]
23. Klimovskikh, I.I.; Otrokov, M.M.; Estyunin, D.; Ereemeev, S.V.; Filnov, S.O.; Koroleva, A.; Shevchenko, E.; Voroshnin, V.; Rybkin, A.G.; Rusinov, I.P.; et al. Tunable 3D/2D magnetism in the (MnBi₂Te₄)(Bi₂Te₃)_m topological insulators family. *npj Quantum Mater.* **2020**, *5*, 54. [[CrossRef](#)]
24. Adachi, Y.; Yuzuri, M.; Kaneko, T.; Abe, S.; Yoshida, H. Magnetic Phase Transition of Cr₂Se₃. *J. Phys. Soc. Jpn.* **1994**, *63*, 369. [[CrossRef](#)]
25. Yang, S.; Feng, C.; Spence, D.; Hindawi, A.M.A.A.; Latimer, E.; Ellis, A.M.; Binns, C.; Peddis, D.; Dhese, S.S.; Zhang, L.; et al. Robust Ferromagnetism of Chromium Nanoparticles Formed in Superfluid Helium. *Adv. Mater.* **2017**, *29*, 1604277. [[CrossRef](#)]
26. Lee, Y.F.; Kumar, R.; Hunte, F.; Narayan, J.; Schwartz, J. Microstructure and transport properties of epitaxial topological insulator Bi₂Se₃ thin films grown on MgO (100), Cr₂O₃ (0001), and Al₂O₃ (0001) templates. *J. Appl. Phys.* **2015**, *118*, 125309. [[CrossRef](#)]
27. Otrokov, M.M.; Klimovskikh, I.I.; Bentmann, H.; Estyunin, D.; Zeugner, A.; Aliev, Z.S.; Gaß, S.; Wolter, A.U.; Koroleva, A.V.; Shikin, A.M.; et al. Prediction and observation of an antiferromagnetic topological insulator. *Nature* **2019**, *576*, 416–422. [[CrossRef](#)] [[PubMed](#)]
28. Haazen, P.P.J.; Laloë, J.B.; Nummy, T.J.; Swagten, H.J.M.; Jarillo-Herrero, P.; Heiman, D.; Moodera, J.S. Ferromagnetism in thin-film Cr-doped topological insulator Bi₂Se₃. *Appl. Phys. Lett.* **2012**, *100*, 082404. [[CrossRef](#)]
29. Chang, C.-Z.; Tang, P.; Wang, Y.L.; Feng, X.; Li, K.; Zhang, Z.; Wang, Y.; Wang, L.L.; Chen, X.; Liu, C.; et al. Chemical-potential-dependent gap opening at the Dirac surface states of Bi₂Se₃ induced by aggregated substitutional Cr atoms. *Phys. Rev. Lett.* **2014**, *112*, 056801. [[CrossRef](#)]
30. Abdalla, L.B.; Seixas, L.; Schmidt, T.M.; Miwa, R.H.; Fazzio, A. Topological insulator Bi₂Se₃(111) surface doped with transition metals: An ab-initio investigation. *Phys. Rev. B* **2013**, *88*, 045312. [[CrossRef](#)]
31. Valla, T.; Pan, Z.-H.; Gardner, D.; Lee, Y.S.; Chu, S. Photoemission spectroscopy of magnetic and nonmagnetic impurities on the surface of the Bi₂Se₃ topological insulator. *Phys. Rev. Lett.* **2012**, *108*, 117601. [[CrossRef](#)] [[PubMed](#)]
32. Shrivies, H.J.; Fernández-Salas, J.A.; Hedtke, C.; Pulis, A.P.; Procter, D.J. Regioselective synthesis of C3 alkylated and arylated benzothiophenes. *Nat. Commun.* **2017**, *8*, 14801. [[CrossRef](#)] [[PubMed](#)]
33. Zhong, M.; Li, S.; Duan, H.-J.; Hu, L.-B.; Yang, M.; Wang, R.Q. Effect of impurity resonant states on optical and thermoelectric properties on the surface of a topological insulator. *Sci. Rep.* **2017**, *7*, 3971. [[CrossRef](#)] [[PubMed](#)]
34. Biswas, R.R.; Balatsky, A.V. Impurity-induced states on the surface of 3D topological insulators. *Phys. Rev. B* **2010**, *81*, 233405. [[CrossRef](#)]
35. Black-Schaffer, A.M.; Balatsky, A.V. Subsurface impurities and vacancies in a three-dimensional topological insulator. *Phys. Rev. B* **2012**, *86*, 115433. [[CrossRef](#)]
36. Koyama, M.; Happo, N.; Tamura, M.; Harada, J.; Mihara, T.; Furuta, A.; Nakatake, M.; Sato, H.; Taniguchi, M.; Ueda, Y. Photoemission and ultraviolet inverse-photoemission studies of CrSe with NiAs-type crystal structure. *J. Electron Spectrosc. Relat. Phenom.* **1996**, *78*, 83–86. [[CrossRef](#)]
37. Zhang, Y.; He, K.; Chang, C.-Z.; Song, C.-L.; Wang, L.-L.; Chen, X.; Jia, J.-F.; Fang, Z.; Dai, X.; Shan, W.-Y.; et al. Crossover of the three-dimensional topological insulator Bi₂Se₃ to the two-dimensional limit. *Nat. Phys.* **2010**, *6*, 584–588. [[CrossRef](#)]
38. Ereemeev, S.V.; Vergniory, M.G.; Menshchikova, T.V.; Shaposhnikov, A.A.; Chulkov, E.V. The effect of van der Waal's gap expansions on the surface electronic structure of layered topological insulators. *New J. Phys.* **2012**, *14*, 113030. [[CrossRef](#)]
39. Aliev, Z.S.; Amiraslanov, I.R.; Nasonova, D.I.; Shevelkov, A.V.; Abdullayev, N.A.; Jahangirli, Z.A.; Orujlu, E.N.; Otrokov, M.M.; Mamedov, N.T.; Babanly, M.B.; et al. Novel ternary layered manganese bismuth tellurides of the MnTe-Bi₂Te₃ system: Synthesis and crystal structure. *J. Alloys Compd.* **2019**, *789*, 443–450. [[CrossRef](#)]
40. Deng, Y.; Yu, Y.; Shi, M.Z.; Guo, Z.; Xu, Z.; Wang, J.; Chen, X.H.; Zhang, Y. Magnetic-field-induced quantized anomalous Hall effect in intrinsic magnetic topological insulator MnBi₂Te₄. *Science* **2020**, *367*, 895–900. [[CrossRef](#)]
41. Rauch, T.; Flieger, M.; Henk, J.; Mertig, I.; Ernst, A. Dual topological character of chalcogenides: Theory for Bi₂Te₃. *Phys. Rev. Lett.* **2014**, *112*, 016802. [[CrossRef](#)] [[PubMed](#)]

Disclaimer/Publisher's Note: The statements, opinions and data contained in all publications are solely those of the individual author(s) and contributor(s) and not of MDPI and/or the editor(s). MDPI and/or the editor(s) disclaim responsibility for any injury to people or property resulting from any ideas, methods, instructions or products referred to in the content.